First-principles insights on phase stability of titanium interstitial alloys

N. S. Harsha Gunda and Anton Van der Ven*
Materials Department, University of California Santa Barbara, Santa Barbara, California 93106, USA

(Received 31 May 2018; published 7 August 2018)

Titanium can dissolve unusually high concentrations of interstitial elements such as carbon and nitrogen to form a rich variety of compounds with beneficial structural and functional properties. A first-principles statistical mechanics study was performed to predict phase stability in the Ti-C and Ti-N binaries. Density functional theory calculations were combined with the cluster-expansion approach to determine ground-state carbon-vacancy and nitrogen-vacancy orderings over the octahedral sites of hcp and fcc Ti. A large number of vacancy-ordered rocksalt phases were found to be stable at low temperature. Monte Carlo simulations showed that the ordered rocksalts transform to a disordered rocksalt that can tolerate high vacancy concentrations at intermediate to high temperatures. Clear trends in phase stability, rooted in electronic structure, are revealed upon a comparison of the calculated Ti-C and Ti-N phase diagrams with the Ti-O phase diagrams from a previous study [N. S. H. Gunda *et al.*, Phys. Rev. Mater. **2**, 033604 (2018)].

DOI: 10.1103/PhysRevMaterials.2.083602

I. INTRODUCTION

Titanium alloys are lightweight and high-strength metals, making them the default option for a diverse number of weight-sensitive structural applications [1]. Titanium is also highly reactive, especially with interstitial elements such as oxygen [2,3], nitrogen [4], and carbon [5]. In fact, a rich variety of compounds with both structural and functional applications can be formed by combining titanium with interstitial elements.

TiC, for example, has a high strength and a high melting point, making it an excellent structural material for coatings, tools, and wear-resistant applications [6]. It is often used in making cermets (ceramic and metal composites), which have attractive mechanical properties [6]. Ti-N compounds also have well-known structural applications and can serve as coatings for tools where wear resistance is a key requirement [7]. Furthermore, the unique optical properties of TiN make it suited for photovoltaic applications [8]. TiN is used as nanoprecipitates in dye-sensitized solar materials [9] and can serve as a plasmonic material to help increase light-trapping efficiency [10]. It is also used as a catalyst to improve the hydrogen-storage efficiency of light-metal complex hydrides [11].

In spite of their numerous structural and functional applications, there are many unknowns about the low-temperature thermodynamic properties of the compounds that form in the Ti-rich half of the Ti-C and Ti-N binaries. Similar to oxygen, both C and N can dissolve interstitially in the hcp crystal structure of Ti. Rocksalt-based carbides and nitrides become stable at equiatomic compositions, with Ti forming an fcc sublattice and C or N filling interstitial octahedral sites. The rocksalt-based TiC and TiN compounds, however, are able to tolerate high concentrations of vacancies on the C or N sublattices. Experimentally very little is known about the low-temperature ordering tendencies of the vacancies and their order-disorder transitions.

Here, we report on a comprehensive first-principles statistical mechanics study of phase stability at finite temperature in the Ti-C and Ti-N binary systems. We identify low-temperature C-vacancy and N-vacancy orderings over the octahedral sites of hcp and fcc Ti and explore their order-disorder transitions with cluster-expansion approaches and Monte Carlo simulations. We compare calculated temperature versus composition phase diagrams with those of a similar study of the Ti-O binary [12] to identify trends in the Ti-*X* phase stability upon increasing the number of valence electrons when *X* goes from C to N to O. The high interstitial solubility of C, N, and O in hcp and fcc Ti is rooted in the peculiar electronic structure of these compounds.

II. METHODOLOGY

Temperature-dependent thermodynamic properties of Ti-*X* systems, with *X* being carbon (C) or nitrogen (N), were calculated by combining first-principles electronic structure methods with statistical mechanics approaches. Density functional theory (DFT) as implemented in the VASP package [13–16] was used to calculate the zero Kelvin energies of a large number of C and N orderings over the octahedral interstitial sites of hcp and fcc Ti. These energies served as training data to parametrize cluster-expansion Hamiltonians [17–19], which are capable of describing the configurational energy of a crystal with near first-principles accuracy. The expansion coefficients were determined with least-squares regression techniques combined with a genetic algorithm to select an optimal set of cluster expansion basis functions [20].

The cluster expansions were implemented in grand-canonical Monte Carlo simulations to calculate thermodynamic quantities as a function of temperature and chemical potential. Free-energy descriptions of the various phases as a function of temperature and composition were obtained

*avdv@ucsb.edu

with standard free-energy integration techniques applied to Monte Carlo generated data [21–23]. The CASM software package [24–27] was used to enumerate symmetrically distinct orderings, to construct and parametrize cluster-expansion Hamiltonians, and to perform Monte Carlo simulations.

The first-principles calculations were performed within the generalized gradient approximation of Perdew, Burke and Ernzerhof (DFT-PBE) [28,29] using the projector augmented wave (PAW) method [30,31] to describe interactions between core and valence electrons. The PAW potentials treat the $3s$, $3p$, $3d$, and $4s$ orbitals of Ti (Ti-sv) and the $2s$ and $2p$ orbitals of C and N as valence states. The plane-wave expansion of the electronic states had an energy cutoff of 550 eV. A $15 \times 15 \times 9$ ($16 \times 16 \times 8$) k-point grid was found to achieve convergence within a 2 meV/unit cell for the primitive cell of the hcp Ti-C (Ti-N) system. A $17 \times 17 \times 17$ k-point grid was used for the primitive cell of rocksalt-based Ti-C and Ti-N compounds. These k-point grids were centered around the Γ point and were scaled appropriately for supercells of the primitive unit cells. Each structure was fully relaxed with respect to lattice parameters and atomic coordinates. Partial occupancy during relaxation runs was treated with the Methfessel-Paxton scheme (of order 2), while the tetrahedron method with Blöchl corrections was used during the static runs. All the ground states predicted in the current study relaxed to a nonmagnetic state when starting from a ferromagnetically initialized configuration.

III. GROUND-STATE ANALYSIS

The search for ground-state C-vacancy and N-vacancy orderings over the octahedral interstitial sites of hcp and fcc Ti was performed iteratively. The energies of an initial set of orderings within a particular parent crystal structure (i.e., hcp Ti or fcc Ti) were first calculated with DFT-PBE and used to train cluster-expansion Hamiltonians for each parent crystal. The cluster expansions were then used to calculate the energies of a substantially larger set of orderings. Any cluster-expansion-predicted low-energy configurations that were not part of a previous training set were then included in a next batch of configurations whose energies were calculated with DFT-PBE. The iterative process was continued until the cluster expansions no longer predicted new ground-state configurations.

The formation energies of most orderings in the Ti-C binary are negative when calculated relative to Ti and graphite. Experimental phase diagrams indicate that rocksalt TiN forms relative to Ti and N_2 gas [4]. To reveal subtle energy differences between the many low-energy orderings, we use hcp Ti and hcp TiX (where X=C or N fills all octahedral interstitial sites) as reference states. The calculated formation energies for the different configurations are shown in Fig. 1(a) for the Ti-C system and in Fig. 1(b) for the Ti-N system. As a measure of composition, we use atomic fractions defined as $y = N_X/(N_{Ti} + N_X)$, where N_{Ti} and N_X are the number of Ti and X atoms, respectively. The value of y varies from 0 to 0.5 for configurations having compositions between Ti and TiX. The formation energy per atom, $E_f(y)$, for a configuration having a composition y (i.e., $Ti_{1-y}X_y$), is then defined as

$$E_f(y) = E(y) - (1-2y)E[\mathrm{Ti}] - (y)E[\mathrm{Ti}X], \qquad (1)$$

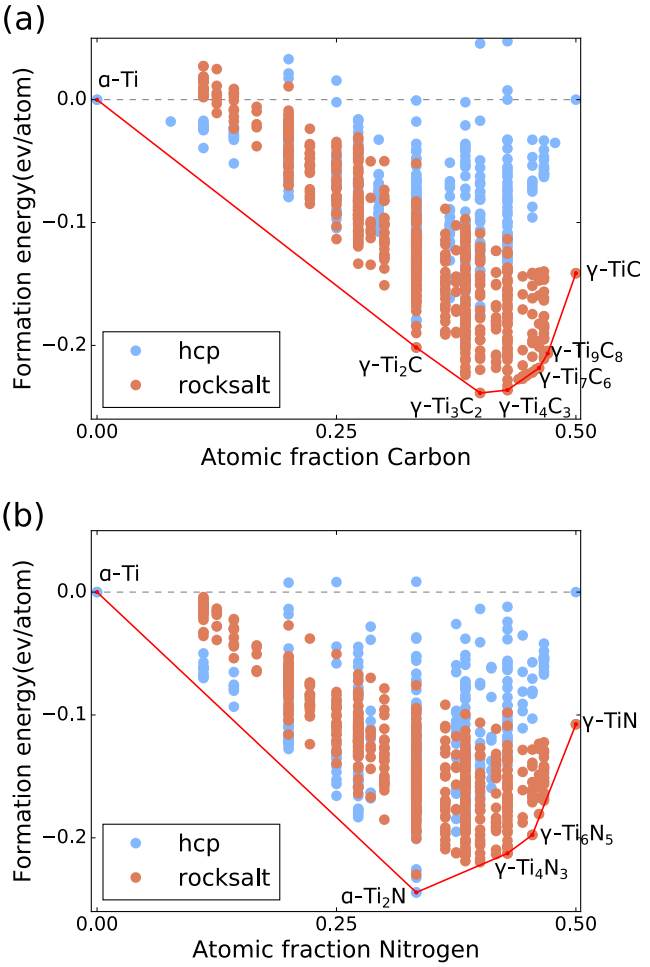

FIG. 1. Formation energies of enumerated configurations in (a) the Ti-C binary and (b) the Ti-N binary. The red line corresponds to the global convex hull and connects the energies of the ground-state orderings.

where $E(y)$ is the energy of the configuration $Ti_{1-y}X_y$, E[Ti] is the energy of hcp Ti, and E[TiX] is the energy of hcp Ti with X filling all the octahedral sites.

The global convex hulls in Figs. 1(a) and 1(b) show that both the Ti-C and Ti-N systems have a series of ground states that are stable at 0 K [32]. Figure 2 illustrates the various ground-state orderings. It is interesting to note that all the ground states are of the type Ti_nX_{n-1} with $n > 1$, although not all integer values of n correspond to ground-state stoichiometries.

Both fcc and hcp consist of close-packed triangular layers having an ABC and an ABAB stacking, respectively. The interstitial octahedral sites of fcc also form an fcc lattice. The interstitial octahedral sites of hcp form a simple hexagonal lattice in which triangular layers of octahedral sites stack in a CCC sequence between the ABAB close-packed layers of the hcp crystal. Figure 2 illustrates the different ground-state orderings as two-dimensional stackings of close-packed layers. The relaxed coordinates of each ground state are also provided in the Supplemental Material [33]. We describe the orderings of Fig. 2 in the next two sections.

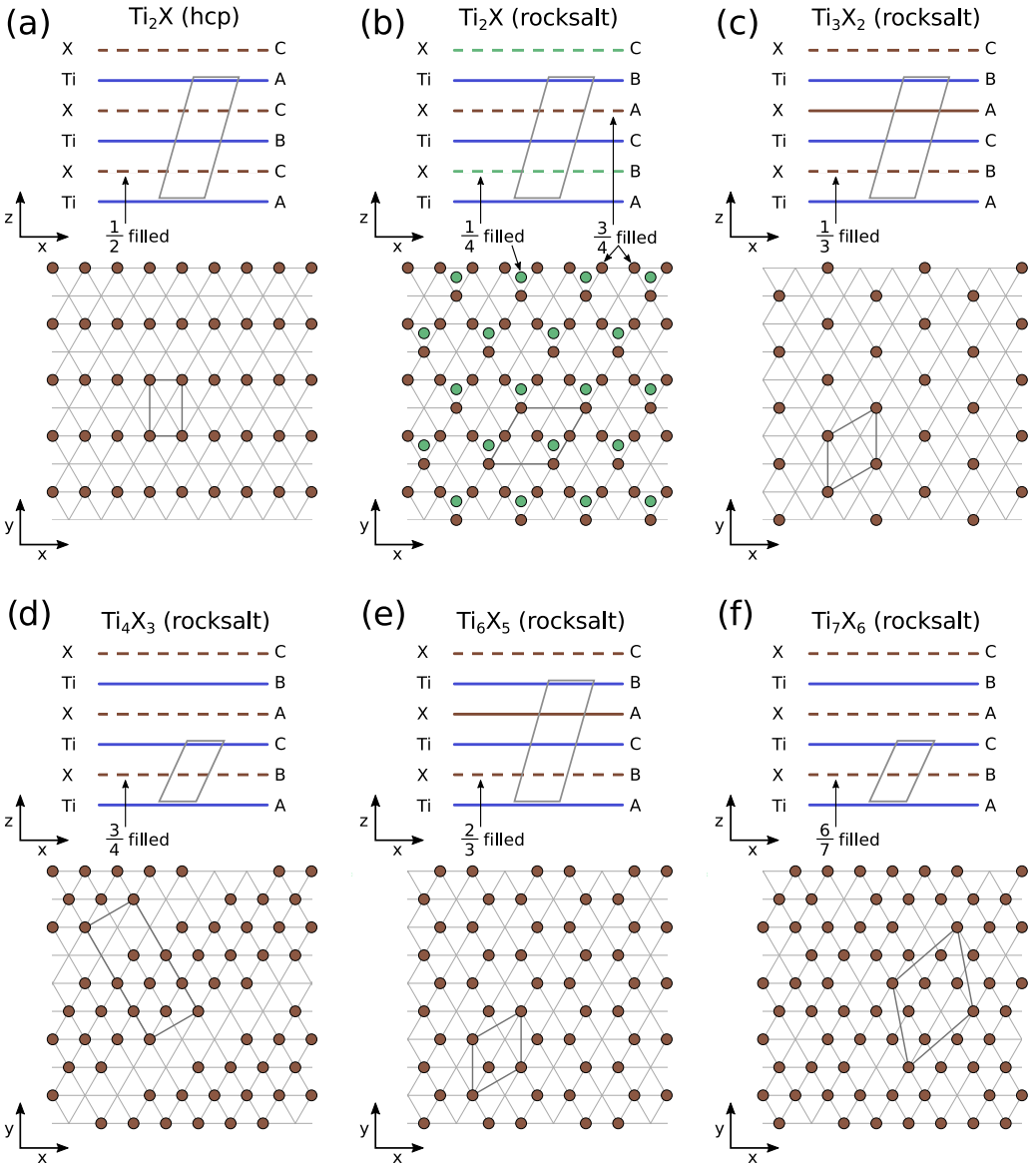

FIG. 2. Interstitial-vacancy orderings within the ground states of the Ti-N and Ti-C binaries. Each ground-state ordering can be generated by a particular stacking of two-dimensional interstitial-vacancy ordered layers. The top half of each subfigure shows the stacking of alternate metal and interstitial layers along the c axis of hcp or along a (111) direction of fcc. Dashed lines indicate close-packed layers containing interstitial vacancies, while solid lines indicate completely filled layers. The bottom half of each subfigure shows the ordering of interstitial atoms over the triangular close-packed planes of octahedral sites in hcp and fcc. The black (gray) boxes shows the unit cell of the ordered ground states.

A. Ti-C binary system

We enumerated 477 (645) C-vacancy configurations over the octahedral sites of hcp Ti (fcc Ti) in supercells having volumes up to six (nine) times that of the primitive unit cell. The formation energies of Fig. 1(a) show that only fcc Ti-derived configurations with high carbon concentrations reside on the convex hull. There are no hcp-based ground-state orderings. The stoichiometric formulas for the ground states are Ti_2C, Ti_3C_2, Ti_4C_3, Ti_7C_6, Ti_9C_8, and the pure rocksalt structure TiC at equiatomic composition. The experimental literature refers to rocksalt TiC as the γ phase [34,35]. We will use the prefix γ to indicate that a particular stoichiometry corresponds to a vacancy-ordered rocksalt phase.

The γ-Ti_2C ground-state ordering is shown in Fig. 2(b) and has cubic symmetry. The carbon concentration fluctuates between 3/4 and 1/4 in alternating (111) octahedral layers. The carbon ordering over the octahedral sites of fcc Ti in γ-Ti_2C is identical to that of the Al cations over the octahedral sites of the fcc oxygen sublattice of spinel $MgAl_2O_4$. The γ-Ti_3C_2 ground state shown in Fig. 2(c) consists of alternating octahedral (111) layers within fcc Ti that are 1/3 filled and fully filled. The carbon in the 1/3-filled layers order on a $\sqrt{3}a \times \sqrt{3}a$ superlattice, which is a common ordering on the triangular lattice. This ordering maximizes the distance between carbon atoms within the 1/3-filled (111) layer.

The γ-Ti_4C_3 ground state shown in Fig. 2(d) has a uniform 3/4 filling in each (111) plane of octahedral interstitial sites.

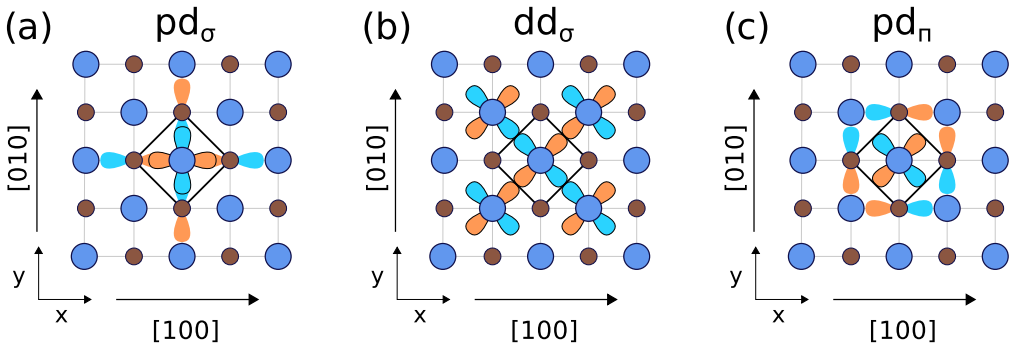

FIG. 3. The orientation of metal host d orbitals and interstitial p orbitals in (a) pd_σ, (b) dd_σ, and (c) pd_π bonds projected on a (100) plane of conventional rocksalt unit cell.

The vacancies order into zigzag rows separated by three zigzag rows of carbon atoms. The γ-Ti_7C_6 ground state shown in Fig. 2(f) has a uniform distribution of carbon in every (111) plane with vacancies ordering on a $\sqrt{7}a \times \sqrt{7}a$ superlattice. This superlattice ordering maximizes the distance between vacancies within each (111) layer when one out of every seven sites are vacant.

The final rocksalt-derived ground state identified here with stoichiometry γ-Ti_9C_8 has a very dilute vacancy concentration. It consists of two completely filled (111) layers alternated by a 2/3-filled (111) layer in which the vacancies order on a $\sqrt{3}a \times \sqrt{3}a$ superlattice. This ground-state ordering is only marginally stable, barely breaking the common tangent between γ-Ti_7C_6 and stoichiometric γ-TiC.

B. Ti-N binary system

For the Ti-N system, we enumerated 393 (630) N-vacancy orderings over the octahedral sites of hcp (fcc) Ti in supercells up to volume five (nine) of the primitive cell. In contrast to the Ti-C system, there is one hcp-based ground state having a stoichiometry of Ti_2N in the Ti-N system. The ground-state ordering of Ti_2N is shown in Fig. 2(a). Every triangular layer of octahedral interstitial sites is half filled, with nitrogen ordering in rows separated by rows of vacancies. The in-plane row orderings in adjacent layers are translated relative to each other such that nitrogen atoms never share faces with each other. Experimental phase diagrams show the existence of an hcp-based compound with a Ti_2N composition [4] and the ordering of nitrogen atoms match the first-principles-derived ground state.

The Ti-N system also has two rocksalt-derived ground states having stoichiometries γ-Ti_4N_3 and γ-Ti_6N_5, where as before we use γ to denote that the compounds are derived from rocksalt. The nitrogen ordering within γ-Ti_4N_3 is identical to that of γ-Ti_4C_3 and is illustrated in Fig. 2(d). The γ-Ti_6N_5 ground state consists of completely filled (111) layers of octahedral interstitial sites alternated by 2/3-filled (111) layers. The nitrogen vacancies in the 2/3-filled layers order on a $\sqrt{3}a \times \sqrt{3}a$ superlattice.

IV. ELECTRONIC STRUCTURE

We next analyze the electronic structure of the ground-state orderings of the previous section. To reveal trends, we compare density of states plots of the Ti-C and Ti-N ground-state orderings to those of similar Ti-O orderings. The three interstitial species, C, N, and O, are neighbors in the periodic table, having the same valence shell, but differing in their number of valence electrons and nuclear charge.

The electronic structure of the rocksalt forms of TiO, TiN, and TiC is well understood [36–38]. Each Ti atom in a rocksalt TiX phase is coordinated by an octahedron of X. The cubic symmetry of the rocksalt crystal structure breaks the degeneracy of the Ti d orbitals into t_{2g} levels (d_{xy}, d_{yz}, and d_{xz} orbitals) and e_g levels ($d_{x^2-y^2}$ and d_{z^2} orbitals). Figure 3 shows the orientation of these orbitals along with the p orbitals of the interstitial atoms on a (100) plane of the conventional rocksalt unit cell. The on-axis e_g orbitals point towards interstitial atoms and can hybridize with their p orbitals to form pd_σ bonds [Fig. 3(a)]. The off-axis t_{2g} orbitals point towards the neighboring Ti atoms to form dd_σ bonds [Fig. 3(b)]. They also form pd_π bonds with the p orbitals of the interstitial elements [36], as can be seen in Fig. 3(c).

Figure 4 compares the calculated electronic density of states of fcc-Ti with those of rocksalt TiO, TiN, and TiC. The density of states have been aligned using the core Ti 3s states. The energy levels of the 3s states are sufficiently deep that they are negligibly affected by the surrounding environment. In addition to showing the total density of states, Fig. 4 also shows projected densities of states, with contributions from Ti t_{2g} (e_g) levels shown in green (orange) and contributions from X p levels shown in light green.

The insertion of O, N, and C into the interstitial sites of fcc Ti to form rocksalt introduces p states well below the Fermi level (Fig. 4). The p levels progressively increase in energy due to a decrease in nuclear charge when going from O to N to C. The p states hybridize with the Ti d orbitals to form bonding pd_σ and pd_π states below the Fermi level and antibonding pd_σ^* and pd_π^* above the Fermi. Since the oxygen p states are much lower than the Ti d states, there is little hybridization and the bonding pd_σ and pd_π states in TiO are primarily of p character localized on oxygen. The p levels of nitrogen are slightly higher than those of oxygen, leading to more hybridized bonding pd_σ and pd_π states in TiN. The carbon p levels appear at even higher energies, allowing for significant overlap with the Ti d orbitals to produce clearly hybridized pd_σ and pd_π bonds in TiC.

Shifts in the intrinsic p levels and number of valence electrons when going from O to N to C also results in clear

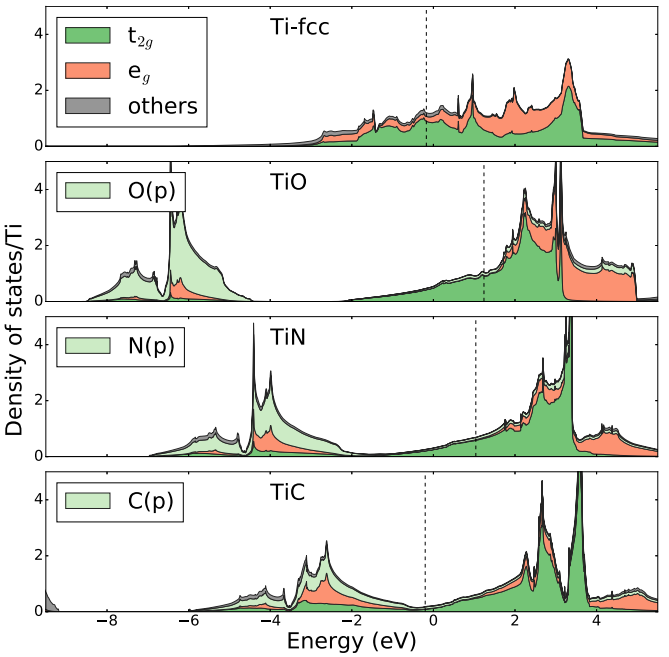

FIG. 4. Projected density of states of fcc-Ti and rocksalt-TiX (X=C,N,O) compounds.

variations in the electronic structure at the Fermi level. In fcc-Ti, there are no interstitial atoms and the states below the Fermi level are predominantly t_{2g} in character, suggesting the importance of directional dd_σ bonds between neighboring Ti atoms. Similar to fcc Ti, the levels at and immediately below the Fermi level in TiO and TiN also have t_{2g} character. The Fermi energy in TiC, in contrast, lies in a shallow valley separating the bonding pd_σ and pd_π states between Ti and C from the Ti d states having t_{2g} character. Bonding in TiC is, therefore, predominantly between Ti and C, with the majority of t_{2g} states necessary for dd_σ bonds residing above the Fermi level and unoccupied.

The introduction of vacancies into the rocksalt forms of TiO, TiN, and TiC results in "vacancy states" below the Fermi level [39,40]. These emerge from a realignment of d orbitals of the Ti atoms next to interstitial vacancies. Figure 5 shows the density of states in substoichiometric Ti_2X rocksalt-based compounds. The interstitial vacancy ordering is identical to that of the Ti_2C ground-state configuration of Fig. 2(b). The presence of vacancies does not qualitatively modify the nature of hybridization between Ti and interstitial atoms that is evident in perfect rocksalt. However, new states in the density of states appear in the vicinity of the Fermi level. The removal of interstitial atoms from perfect rocksalt results in the partial elimination of Ti-X pd_σ and pd_π bonds, which is then compensated by a strengthening of the dd_σ bonds between neighboring Ti [41]. This is evident in Fig. 5 from the dominance of t_{2g} character in the peaks corresponding to vacancy states.

Figure 6 shows the effect of changes in the vacancy concentration on the density of states of TiC_x. Each compound in Fig. 6 corresponds to a vacancy-ordered rocksalt ground state in the Ti-C binary. While the qualitative features of the interstitial/metal hybridization below the Fermi level does

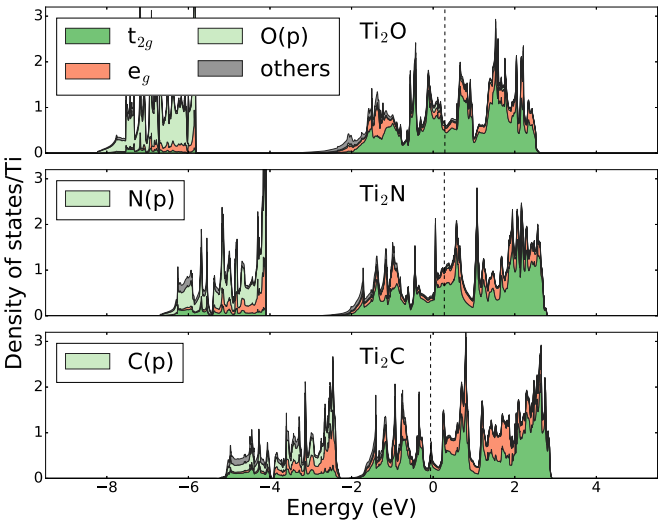

FIG. 5. Projected density of states of rocksalt-Ti_2X (X=C,N,O) compounds.

not change, more and more vacancy states emerge below the Fermi level with vacancy concentration. Furthermore, the peaks associated with the new states along with other states become sharper when going from TiC to Ti_2C, indicating an increase in localization. The introduction of C vacancies reduces the number of Ti-C bonds that draw electrons from the Ti host, allowing for the filling of Ti d levels that have predominantly t_{2g} character.

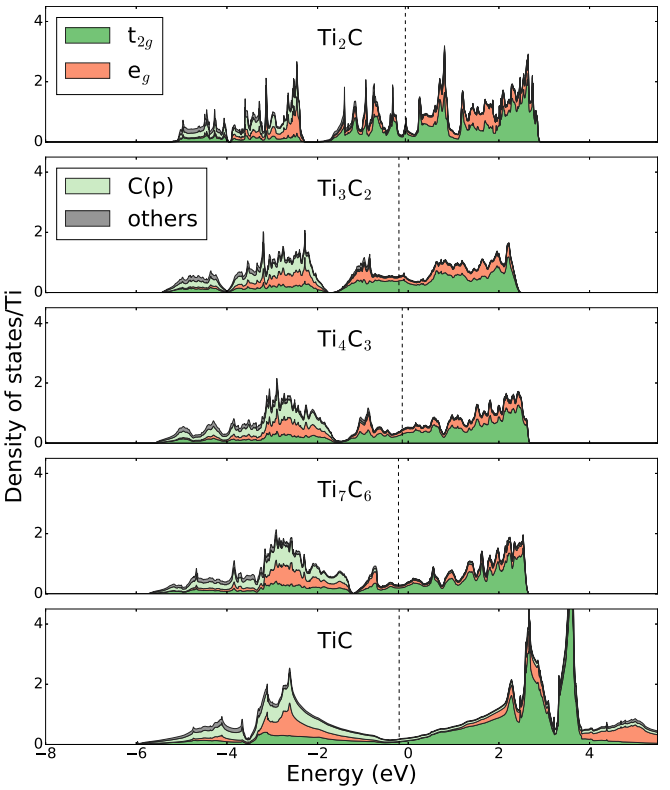

FIG. 6. Projected density of states of ground-state rocksalt titanium carbides.

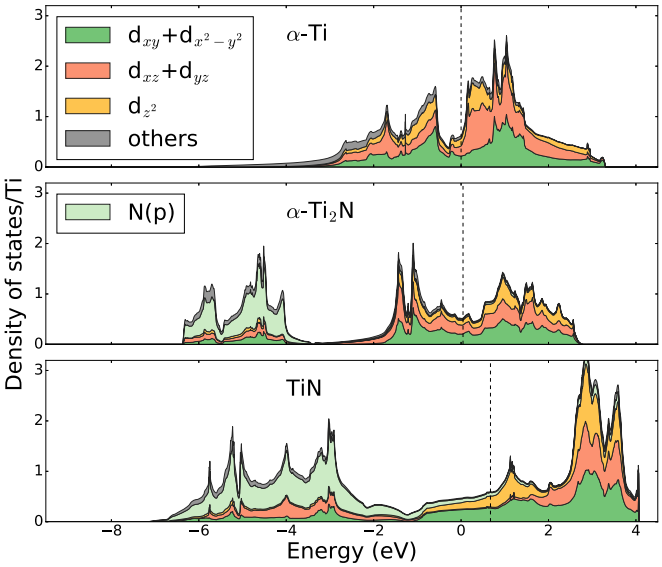

FIG. 7. Projected density of states of α-Ti, the α-Ti_2N ground state, and metastable hcp TiN.

Bonding in the hcp-based compounds is more subtle than in the cubic rocksalt phases. The hexagonal symmetry of hcp splits the d orbitals into three symmetrically distinct groups. One corresponds to the d_{z^2} orbital with lobes aligned along the z axis. The second group consists of combinations of d_{xy} and $d_{x^2-y^2}$ to yield orbitals that point towards Ti nearest neighbors within the close-packed planes. The remaining d_{yz} and d_{xz} orbitals point out of the x-y plane and can hybridize with the Ti of adjacent close-packed planes. It is well known that the early transition metals Ti, Zr, and Hf are stable in the hcp crystal structure at low temperature since their Fermi level resides within a valley in the electronic densities of state of the transition-metal d levels [42]. This is evident in Fig. 7(a).

Figure 7(b) shows the density of states in the hcp-based α-Ti_2N ground state [Fig. 2(a)], while Fig. 7(c) shows that of metastable hcp-TiN. The interstitial octahedral sites in hcp form a trigonal prism around the host metal atoms. The p orbitals of the interstitial species can hybridize with the d_{yz} and d_{xz} orbitals of Ti to form σ bonds and with the d_{xy} and $d_{x^2-y^2}$ to form π bonds [43]. Figures 7(b) and 7(c) indicate that such hybridization does indeed occur in α-Ti_2N and hcp TiN. In fact, the partial densities of states in Figs. 7(b) and 7(c) are qualitatively similar to those of the rocksalt phases, with bonding states between N p levels and Ti d levels appearing below the Fermi level, and with Ti d states dominating at and immediately below the Fermi level.

V. PHASE DIAGRAMS

Predicting phase stability at finite temperature requires a statistical mechanics approach [18,19]. The formation energies for the Ti-C and Ti-N binaries were used to parameterize cluster expansions of the configurational energy [44]. These were then implemented in grand-canonical Monte Carlo simulations to calculate the free energies needed to construct temperature versus composition phase diagrams. The average interstitial concentration and average grand-canonical energy were calculated with grand-canonical Monte Carlo simulations over a grid of temperatures and interstitial chemical potentials. Standard free-energy integration techniques [21–23] were then applied to this data to calculate free energies as a function of interstitial composition over a range of temperatures. The phase diagrams were subsequently constructed using the common tangent method to map out two-phase coexistence regions.

Figures 8(a) and 8(b) show the calculated phase diagrams for the Ti-C and the Ti-N binaries, respectively. For comparison, Fig. 8(c) shows a phase diagram of the Ti-O binary calculated using similar approaches [12]. Not included in the phase diagrams of Fig. 8 is the high-temperature bcc phase. This phase is stabilized by vibrational entropy and only appears at high temperature. The neglect of the high-temperature bcc phase does not affect our predictions of carbide and nitride phase stability at intermediate to low temperatures. The hcp interstitial solid solutions are shown in light blue, while any hcp-derived ordered phase is shown in dark blue. The disordered rocksalts (i.e., X-vacancy disorder over the interstitial octahedral sites of fcc Ti) are shown in light orange, while any vacancy-ordered rocksalt phases are shown in light brown.

Figures 8(a) and 8(b) show an appreciable solubility of C and N in hcp Ti. The N solubility is substantially higher than that of C. A comparison of Figs. 8(a) and 8(b) to Fig. 8(c) reveals that oxygen has an even higher solubility in hcp Ti than both N and C. At 1200 K, for example, the solubility in hcp Ti is 5% for C, increasing to 20% for N, and going as high as 33% for O. The number of hcp-derived ordered phases also increases when going from C to N to O. In the Ti-C binary, there are no hcp-based ordered phases. In the Ti-N binary, in contrast, the hcp-based ordered Ti_2N phase [Fig. 2(a)] is predicted be stable to very high temperatures, transforming to a disordered rocksalt around 1900 K. The Ti-O binary has even more hcp-derived ordered phases with stoichiometries Ti_6O, Ti_3O, and Ti_2O. These suboxide phases disorder to an hcp Ti-O solid solution at around 1000 K.

The rocksalt phase is predicted to be stable over a wide concentration interval in both the Ti-C and Ti-N systems. Most of the ground-state vacancy orderings in the Ti-C and Ti-N rocksalts remain stable to quite high temperatures, disordering at temperatures that range between 600 and 1400 K. Only the γ-Ti_9C_8 vacancy-ordered rocksalt phase is predicted to have its order/disorder transformation temperature below 400 K and hence it does not appear in the phase diagram shown in Fig. 8(a). The disordered rocksalt phases, labeled γ-TiC and γ-TiN, are stable over wide concentration intervals at elevated temperature, indicating that the carbide- and nitride-based rocksalts are able to tolerate high concentrations of C and N vacancies. Rocksalt-derived phases in the Ti-O binary, in contrast, are only stable in a very narrow concentration interval. In fact, a comparison of Figs. 8(a)–8(c) reveals that the concentration interval in which the rocksalt phase is predicted to be stable progressively decreases when going from C to N to O.

VI. DISCUSSION AND CONCLUSION

The results of this first-principles study has shown that the the Ti-C and Ti-N phase diagrams are substantially more

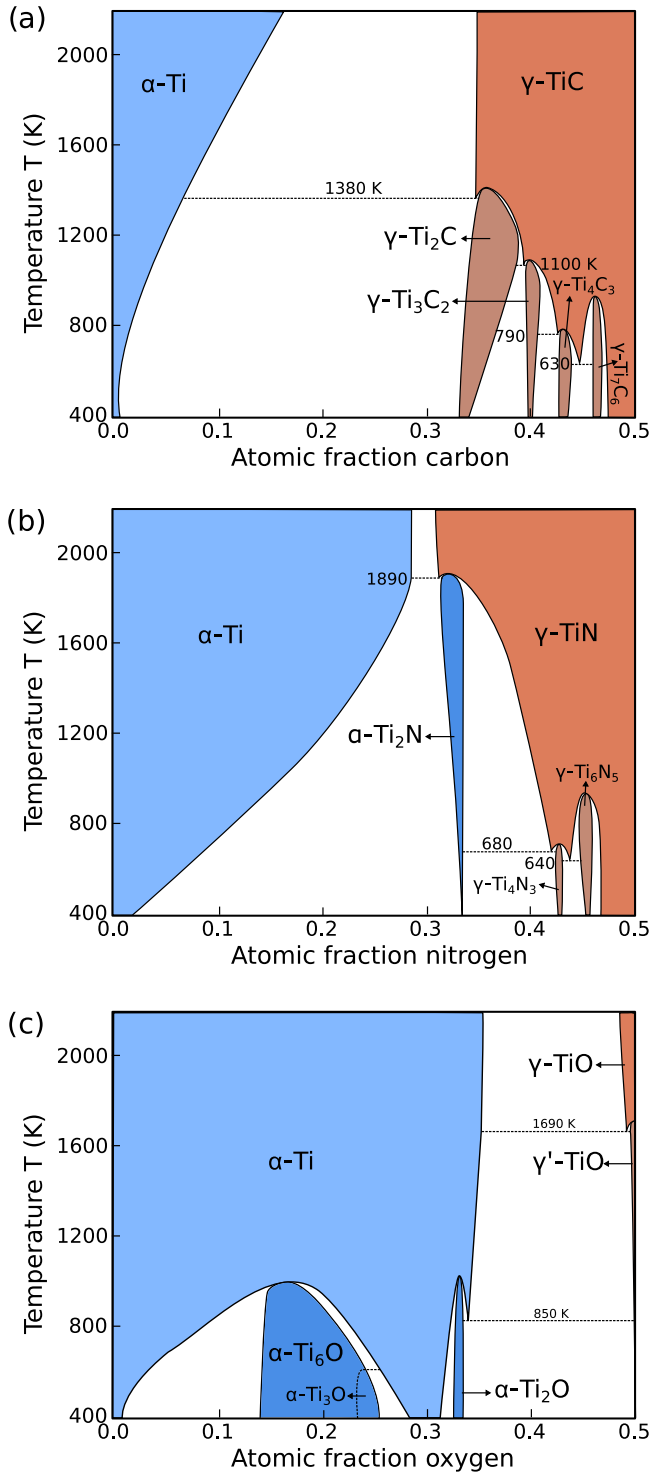

FIG. 8. Computed phase diagrams for the (a) Ti-C, (b) Ti-N, and (c) Ti-O binary systems. Single phase regions colored in shades of blue have an hcp parent crystal and those colored in shades of red are rocksalt based.

complex than is generally assumed based on experimental assessments [4,5]. Although there are phase diagrams available in the literature [45,46] that attempt to resolve the stability domains of Ti-C vacancy-ordered hcp and rocksalt phases, they do not contain many of the ground states predicted here and previously [47]. DFT-PBE predicts a large number of vacancy-ordered ground states, especially within the TiC_x and TiN_x rocksalt phases. The ordering of γ-Ti_2C has been determined experimentally [48] and matches that predicted in this study. Several other ground states have been predicted previously from first principles. These include the vacancy orderings in Ti_3C_2 and Ti_7C_6 [49,50] and the Ti_6N_5 ground-state ordering [51]. A ground-state vacancy ordering has also been predicted for Ti_4N_3 [51]; however, insufficient crystallographic detail was provided to enable a comparison with the ground state of this study at the same composition. Ground states discovered in this study include γ-Ti_4C_3 and γ-Ti_9C_8.

The calculated temperature-composition phase diagrams of Fig. 8 show that the vacancy-ordered rocksalt phases remain stable to high temperatures. Consistent with experimental observations [4,5], the disordered TiC_x and TiN_x rocksalt phases can tolerate very high vacancy concentrations on the C and N sublattices, respectively. Although our calculations have rigorously accounted for configurational degrees of freedom, they did not include contributions from vibrational excitations [52,53]. The inclusion of vibrational excitations may alter the predicted transition temperatures; however, they are unlikely to modify the qualitative phase relations predicted in this work.

As is evident from Fig. 1, titanium has a remarkable ability to dissolve large atom fractions of C, N, and O within the octahedral sites of hcp and fcc. All three interstitial elements form bonding states (pd_σ, pd_π) and antibonding states (pd^*_σ, pd^*_π) upon hybridization with Ti d levels. The bonding states appear well below the Fermi level and are consequently completely filled (Figs. 4 and 7). This ability to fill the bonding states and leave the high-energy antibonding states unoccupied is one factor contributing to the high solubility of interstitial atoms in hcp and fcc Ti.

All three Ti-X (X=C, N, and O) binaries favor an hcp Ti host at low interstitial concentrations and an fcc host at high concentrations (Fig. 8). This trend likely has its origin in crystallographic differences between hcp and fcc. The octahedral interstitial sites of hcp Ti share faces with each other, while those of fcc Ti only share edges. Below the Ti_2X stoichiometry, the interstitial-vacancy orderings within hcp Ti minimize energy by avoiding simultaneous occupancy of pairs of face-sharing octahedral sites. This becomes more difficult in hcp above the Ti_2X stoichiometry, and the rocksalt phases with an fcc Ti sublattice become more stable.

Figures 8(a)–8(c) reveal a clear trend in the relative stability between hcp and rocksalt phases at intermediate interstitial compositions, with the rocksalt phases becoming more stable relative to hcp upon going from O to N to C. This behavior is likely rooted in the electronic structure that emerges upon insertion of interstitial elements into hcp and fcc Ti. The electronic levels at and immediately below the Fermi levels of the Ti-X compounds are dominated by Ti d states. More of these states are occupied in the Ti-O compounds than in Ti-C compounds with the same structure since O has more valence electrons than C. As a result, bonding pd_σ and pd_π states play a more important role in Ti-C compounds than they do in Ti-O compounds. This difference is likely in part responsible for the higher stability of rocksalt in the Ti-C system than in the Ti-O system. The cubic symmetry of fcc Ti and its

interstitial network is well suited for the pd_σ hybridization that characterizes the TiC_x rocksalt phases. On the other hand, the hcp Ti host of the TiO_x suboxides is more favored when the Ti d states play a more prominent role [42]. The Ti-N compounds have electronic structures that are intermediate to those of the Ti-O and Ti-C compounds. As a consequence, the degree with which rocksalt is favored at intermediate interstitial composition in the Ti-N binary is between that of the Ti-O and Ti-C binaries.

The variation in relative stability between hcp- and fcc-based compounds with the chemical identity of the interstitial guest species can be exploited in synthesis. For example, it is well known that pretreatment of Ti with carbon leads to a surface rocksalt TiC_x precursor phase that favors the subsequent formation of anatase TiO_2 as opposed to rutile TiO_2 upon further oxidation [54]. The presence of N in air means that it plays an important role during the oxidation of Ti. Future work will focus on mixtures of O, N, and C within hcp Ti and rocksalt. It is likely that low-temperature O-N-C-vacancy-ordered phases exist within hcp and fcc Ti with interesting structural and functional properties.

ACKNOWLEDGMENTS

We acknowledge our funding source, NSF DMREF Grant No. DMR1436154 "DMREF: Integrated Computational Framework for Designing Dynamically Controlled Alloy - Oxide Heterostructures." The computations were performed using resources supported by the Center for Scientific Computing, CNSI and MRL under NSF MRSEC (Grant No. DMR-1720256). Computing resources were also provided by the National Energy Research Scientific Computing Center, a U.S. Department of Energy Office of Science User Facility supported by the Office of Science of the U.S. Department of Energy under Contract No. DE-AC02-05CH11231.

[1] R. R. Boyer, Mater. Sci. Eng. A **213**, 103 (1996).
[2] J. L. Murray and H. A. Wriedt, J. Phase Equilib. **8**, 148 (1987).
[3] H. Okamoto, J. Phase Equilib. Diffus. **32**, 473 (2011).
[4] H. A. Wriedt and J. L. Murray, Bull. Alloy Phase Diagr. **8**, 378 (1987).
[5] H. Okamoto, J. Phase Equilib. Diffus. **27**, 306 (2006).
[6] F. P. Knudsen, R. E. Moreland, and R. F. Geller, J. Am. Ceram. Soc. **38**, 312 (1955).
[7] U. Helmersson, B. O. Johansson, J. Sundgren, H. T. G. Hentzell, and P. Billgren, J. Vac. Sci. Technol. A **3**, 308 (1985).
[8] H. Wang, Q. Chen, L. Wen, S. Song, X. Hu, and G. Xu, Photon. Res. **3**, 329 (2015).
[9] C.-T. Li, S.-R. Li, L.-Y. Chang, C.-P. Lee, P.-Y. Chen, S.-S. Sun, J.-J. Lin, R. Vittal, and K.-C. Ho, J. Mater. Chem. A **3**, 4695 (2015).
[10] A. Lalisse, G. Tessier, J. Plain, and G. Baffou, Sci. Rep. **6**, 38647 (2016).
[11] L. Li, F. Qiu, Y. Wang, G. Liu, Y. Xu, C. An, Y. Wang, L. Jiao, and H. Yuan, J. Mater. Chem. **22**, 13782 (2012).
[12] N. S. H. Gunda, B. Puchala, and A. Van der Ven, Phys. Rev. Mater. **2**, 033604 (2018).
[13] G. Kresse and J. Hafner, Phys. Rev. B **47**, 558 (1993).
[14] G. Kresse and J. Hafner, Phys. Rev. B **49**, 14251 (1994).
[15] G. Kresse and J. Furthmüller, Comput. Mater. Sci. **6**, 15 (1996).
[16] G. Kresse and J. Furthmüller, Phys. Rev. B **54**, 11169 (1996).
[17] J. M. Sanchez, F. Ducastelle, and D. Gratias, Physica A (Amsterdam) **128**, 334 (1984).
[18] D. D. Fontaine, Solid State Phys. **47**, 33 (1994).
[19] A. Van der Ven, J. C. Thomas, B. Puchala, and A. R. Natarajan, Annu. Rev. Mater. Res. **48**, 27 (2018).
[20] G. L. W. Hart, V. Blum, M. J. Walorski, and A. Zunger, Nat. Mater. **4**, 391 (2005).
[21] A. van de Walle and M. Asta, Modell. Simul. Mater. Sci. Eng. **10**, 521 (2002).
[22] A. S. Dalton, A. A. Belak, and A. Van der Ven, Chem. Mater. **24**, 1568 (2012).
[23] A. R. Natarajan, J. C. Thomas, B. Puchala, and A. Van der Ven, Phys. Rev. B **96**, 134204 (2017).
[24] CASM, v0.2.0 (2016), available from https://github.com/prisms-center/CASMcode, doi:10.5281/zenodo.60142.
[25] J. C. Thomas and A. Van der Ven, Phys. Rev. B **88**, 214111 (2013).
[26] B. Puchala and A. Van der Ven, Phys. Rev. B **88**, 094108 (2013).
[27] A. Van der Ven, J. C. Thomas, Q. Xu, and J. Bhattacharya, Math. Comput. Simul. **80**, 1393 (2010).
[28] J. P. Perdew, K. Burke, and M. Ernzerhof, Phys. Rev. Lett. **77**, 3865 (1996).
[29] J. P. Perdew, K. Burke, and M. Ernzerhof, Phys. Rev. Lett. **78**, 1396 (1997).
[30] P. E. Blöchl, Phys. Rev. B **50**, 17953 (1994).
[31] G. Kresse and D. Joubert, Phys. Rev. B **59**, 1758 (1999).
[32] The convex hull corresponds to the envelope of the lowest-energy orderings. Any ordering that resides on the convex hull is a stable ground state at zero Kelvin.
[33] See Supplemental Material at http://link.aps.org/supplemental/10.1103/PhysRevMaterials.2.083602 for details about the coordinates of enumerated structures.
[34] D. Bandyopadhyay, R. C. Sharma, and N. Chakraborti, J. Phase Equilib. **21**, 195 (2000).
[35] D. Bandyopadhyay, R. C. Sharma, and N. Chakraborti, J. Phase Equilib. **21**, 179 (2000).
[36] P. Blaha and K. Schwarz, Int. J. Quantum Chem. **23**, 1535 (1983).
[37] H.-R. Trebin and H. Bross, J. Phys. F **14**, 1453 (1984).
[38] A. Neckel, in *The Physics and Chemistry of Carbides, Nitrides and Borides*, edited by R. Freer (Springer, Dordrecht, 1990), pp. 485–511.
[39] J. Redinger, R. Eibler, P. Herzig, A. Neckel, R. Podloucky, and E. Wimmer, J. Phys. Chem. Solids **46**, 383 (1985).
[40] Z. Dridi, B. Bouhafs, P. Ruterana, and H. Aourag, J. Phys.: Condens. Matter **14**, 10237 (2002).
[41] P. Čapková and L. Skála, Phys. Status Solidi B **171**, 85 (1992).
[42] W. A. Harrison, *Electronic Structure and the Properties of Solids*, Dover Books on Physics (Dover, New York, 1989).
[43] M. Kertesz and R. Hoffmann, J. Am. Chem. Soc. **106**, 3453 (1984).

[44] A separate cluster expansion was constructed for each parent crystal structure. The cluster expansion of the configurational energy of C-vacancy (N-vacancy) disorder over the octahedral sites of hcp Ti was parameterized by fitting to the formation energies of 477 (393) configurations using a genetic algorithm. The hcp-based Ti-C (Ti-N) cluster expansion had a weighted root-mean-square (rms) error of 9.3 (9.7) meV/unit cell and weighted cross-validation (cv) score of 13.5 (11.4) meV/unit cell. The cluster expansion of C-vacancy (N-vacancy) disorder in the rocksalt was parameterized with 645 (629) formation energies and had a weighted rms of 5.1 (6.1) meV/unit cell and a weighted cv of 5.9 (7.0) meV/unit cell.

[45] A. I. Gusev and A. A. Rempel, Dokl. Akad. Nauk **332**, 717 (1993).

[46] V. N. Lipatnikov, L. V. Zueva, A. I. Gusev, and A. Kottar, Phys. Solid State **40**, 1211 (1998).

[47] C. R. Weinberger and G. B. Thompson, J. Am. Ceram. Soc. **101**, 4401 (2018).

[48] V. Moisy-Maurice, N. Lorenzelli, C. H. De Novion, and P. Convert, Acta Metallurg. **30**, 1769 (1982).

[49] X.-X. Yu, C. R. Weinberger, and G. B. Thompson, Comput. Mater. Sci. **112**, 318 (2016).

[50] P. A. Korzhavyi, L. V. Pourovskii, H. W. Hugosson, A. V. Ruban, and B. Johansson, Phys. Rev. Lett. **88**, 015505 (2001).

[51] C. R. Weinberger, X.-X. Yu, H. Yu, and G. B. Thompson, Comput. Mater. Sci. **138**, 333 (2017).

[52] B. Fultz, Prog. Mater. Sci. **55**, 247 (2010).

[53] M.-H. Chen, B. Puchala, and A. Van der Ven, Calphad **51**, 292 (2015).

[54] T. Okazumi, K. Ueda, K. Tajima, N. Umetsu, and T. Narushima, J. Mater. Sci. **46**, 2998 (2011).